KANAZAWA-13-03
UT-HET-078

Reconstruction of Inert Doublet Scalars at the International Linear Collider

Mayumi Aoki,[1,2,*] Shinya Kanemura,[3,†] and Hiroshi Yokoya[3,‡]

[1] *Institute for Theoretical Physics, Kanazawa University, Kanazawa 920-1192, Japan*

[2] *Max-Planck-Institut für Kernphysik, Saupfercheckweg 1, 69117 Heidelberg, Germany*

[3] *Department of Physics, University of Toyama, Toyama 930-8555, Japan*

(Dated: February 25, 2022)

arXiv:1303.6191v2 [hep-ph] 19 Aug 2013

Abstract

We study collider signatures for extra scalar bosons in the inert doublet model at the international linear collider (ILC). The inert doublet model is a simple extension of the standard model by introducing an additional isospin-doublet scalar field which is odd under an unbroken Z_2 symmetry. The model predicts four kinds of Z_2-odd scalar bosons, and the lightest of them becomes stable and a candidate of the dark matter as long as it is electrically neutral. Taking into account the constraints from various theoretical and phenomenological conditions, we perform a simulation study for the distinctive signatures of the extra scalars over the standard-model background contributions at the ILC with the center-of-mass energy of $\sqrt{s} = 250$ GeV and 500 GeV. We further discuss observables for determination of the mass of the scalars. We find that the parameter regions which cannot be detected at the large hadron collider can be probed at the ILC.

PACS numbers: 12.60.Fr, 13.66.Hk, 14.80.Ec, 14.80.Fd,

Keywords: Extended Higgs Theory, Electron Positron Colliders

* mayumi@hep.s.kanazawa-u.ac.jp

† kanemu@sci.u-toyama.ac.jp

‡ hyokoya@sci.u-toyama.ac.jp

I. INTRODUCTION

In July 2012, a Higgs-like particle was found at the large hadron collider (LHC) [1, 2]. The particle looks like mostly a Higgs boson in the standard model (SM), but the detail properties of the particle and the whole structure of the Higgs sector have not yet been revealed. It is widely believed that the SM has to be extended, since it cannot explain the dark matter, (tiny) neutrino masses, and the baryon asymmetry in the Universe, etc. Although in the Higgs sector of the SM, only one $\mathrm{SU}(2)_L$-doublet scalar field is introduced, there is no theoretical guideline for this choice. Thus, the Higgs sector may be a solid target to probe new physics beyond the SM.

The inert doublet model (IDM) is one of the simplest extensions of the SM, where an additional $\mathrm{SU}(2)_L$-doublet scalar field is introduced, which is odd under the unbroken Z_2 symmetry [3, 4]. As in the case in the general two Higgs doublet model, four kinds of additional scalars appear as physical states, namely neutral CP-even state (H), neutral CP-odd state (A) and charged scalar states ($H^\pm$), all of which are called inert scalars. Due to the Z_2 symmetry, Yukawa interactions of the inert scalars to SM fermions are forbidden, and the possible flavor-changing neutral current is absent at the tree level. The lightest inert particle (LIP) is stable, because of the Z_2-parity conservation. Therefore, the model provides a dark matter candidate [4–11]. In addition to that, the model has rich phenomenological features such as the electroweak symmetry breaking [12], electroweak phase transition [13–16], radiatively generating neutrino masses by introducing Z_2-odd right-handed neutrinos [17], and leptogenesis [18, 19], etc.

Collider signatures of the inert scalars in the IDM have been studied in the literature [4, 10, 11, 20–23]. In Ref. [21], bounds on the inert scalar masses are obtained by using the experimental results at the LEP II [24–26]. Since the inert scalars do not have QCD interactions, it is not suited to search for them at hadron colliders. Even though the parameter regions where the inert scalars could be discovered at the LHC are pointed out [10, 22, 23], detailed analysis on these scalars such as the precise determination of these masses and quantum numbers would be difficult.

In this letter, we study collider phenomenology for the inert scalars at the international linear collider (ILC). As it is a machinery for precision measurements of Higgs boson properties, the extended Higgs sector can also be investigated in details. We study the characteristic

signatures, corresponding backgrounds and the kinematical observables in the processes of HA associated production as well as H^+H^- pair production. Earlier studies can be found e.g. in Refs. [27, 28] where the charged scalar pair production process is studied in detail, and in Ref. [29] where HA associated production is also studied. On the other hand, our study includes all the available processes and decay modes, and the simulation analysis for the signal and the background contributions with appropriate kinematical cuts. Furthermore, we also discuss the procedure for the mass determination of the inert scalars which can be performed at an early stage of the experiment, and introduce a new observable which could be useful to determine the inert scalar masses more precisely than the variables used in Refs. [28, 29].

The rest of the letter is organized as follows. In Sec. II, we review the inert doublet model and introduce the benchmark points used in our simulation study. Then we present the simulation studies for observing the inert scalars and determining the masses of them in Sec. III. Sec. IV and Sec. V are devoted to discussions and conclusions, respectively. In Appendix, we evaluate a new observable at e^+e^- colliders which is used in our analysis for the mass determination.

II. THE INERT DOUBLET MODEL

In the IDM, the two scalar doublet fields, Φ_1 and Φ_2, have even and odd parity under the Z_2 symmetry, respectively. The most general scalar potential can be written as

$$\begin{aligned} V(\Phi_1,\Phi_2) = {} & \mu_1^2 |\Phi_1|^2 + \mu_2^2 |\Phi_2|^2 + \frac{\lambda_1}{2} |\Phi_1|^4 + \frac{\lambda_2}{2} |\Phi_2|^4 + \lambda_3 |\Phi_1|^2 |\Phi_2|^2 \\ & + \lambda_4 \left|\Phi_1^\dagger \Phi_2\right|^2 + \left\{ \frac{\lambda_5}{2} \left(\Phi_1^\dagger \Phi_2\right)^2 + \text{H.c.} \right\}, \end{aligned} \tag{1}$$

with seven real parameters $(\mu_1^2, \mu_2^2, \lambda_1, \lambda_2, \lambda_3, \lambda_4, \lambda_5)$. We note that the potential is invariant under the CP transformation. The potential has to satisfy theoretical constraints, such as the vacuum stability [3, 30] and the perturbativity [4]. By the vacuum stability at the tree level, the quartic terms are constrained as $\lambda_1 > 0$, $\lambda_2 > 0$, $\sqrt{\lambda_1\lambda_2} + \lambda_3 > 0$, and $\sqrt{\lambda_1\lambda_2} + \lambda_3 + \lambda_4 - |\lambda_5| > 0$ [3]. We consider the case where $\mu_1^2 < 0$, $\lambda_1\mu_2^2 > \lambda_3\mu_1^2$ and $\lambda_1\mu_2^2 > (\lambda_3+\lambda_4+|\lambda_5|)\mu_1^2$ are satisfied [3], so that Φ_2 does not acquire the vacuum expectation

value (VEV) [31] and only Φ_1 plays a role of the "Higgs-boson". By denoting

$$\Phi_1 = \begin{pmatrix} 0 \\ \frac{1}{\sqrt{2}}(v+h) \end{pmatrix}, \quad \Phi_2 = \begin{pmatrix} H^+ \\ \frac{1}{\sqrt{2}}(H+iA) \end{pmatrix}, \tag{2}$$

where v is the VEV, $v = \sqrt{-2\mu_1^2/\lambda_1} (\simeq 246$ GeV), the masses of these scalars are expressed as

$$m_h^2 = \lambda_1 v^2, \tag{3a}$$

$$m_{H^+}^2 = \mu_2^2 + \frac{1}{2}\lambda_3 v^2, \tag{3b}$$

$$m_H^2 = \mu_2^2 + \frac{1}{2}(\lambda_3 + \lambda_4 + \lambda_5)v^2, \tag{3c}$$

$$m_A^2 = \mu_2^2 + \frac{1}{2}(\lambda_3 + \lambda_4 - \lambda_5)v^2. \tag{3d}$$

Thus, the seven parameters in the Higgs potential can be replaced by the VEV v, four masses of the Higgs boson and inert scalars, (m_h, m_{H^+}, m_H, m_A), the scalar self-coupling constant λ_2, and $\lambda_H (\equiv \lambda_3 + \lambda_4 + \lambda_5)$ for example. To force the LIP to be electrically neutral, so that it can be a candidate of the dark matter, $\lambda_4 < |\lambda_5|$ must be satisfied [30]. Depending on the sign of λ_5, either H or A becomes the LIP. Since phenomenological constraints and collider signatures are exchangeable between the two cases, we take H as the LIP ($\lambda_5 < 0$) hereafter.

In this letter, we consider four benchmark points for the masses of inert scalars listed in Table I, which satisfy all the available theoretical and also phenomenological constraints [32]. The bounds on the masses of inert scalars are briefly summarized as follows. By the constraints from dark matter relic abundance and direct searches, the mass of LIP should be $40 \lesssim m_H \lesssim 80$ GeV [5, 7, 10] [1]. For $m_H < 80$ GeV, the mass of the second neutral scalar has to satisfy $|m_A - m_H| < 8$ GeV or $m_A > 100$ GeV, to avoid the bounds from the direct searches at the LEP experiments [21]. The mass differences of inert scalars result into additional contributions [4] to the electroweak S and T parameters. To be consistent with the current experimental data [33],

$$\Delta T \simeq 1.08 \left(\frac{m_{H^\pm} - m_H}{v}\right)\left(\frac{m_{H^\pm} - m_A}{v}\right) = 0.07 \pm 0.08 \tag{4}$$

must be satisfied. In Ref. [10] these constraints are more extensively studied.

[1] There exists a case in which all the scalar masses are heavy (> 500 GeV) and degenerated [5]. However, since collider searches at the ILC are difficult, we don't consider such case in this study.

In the four benchmark points, the mass of H is fixed to 65 GeV, so that it does not induce the invisible decay of the SM Higgs boson. While it could be up to $\sim$ 80 GeV concerning the dark matter relic abundance analysis [5, 7–11], the collider phenomenology does not change qualitatively by varying it in that region. Above that value, $HH \to W^+W^-$ process gives a too large annihilation cross section, so that the predicted relic density in the IDM results into a lower value than that from the WMAP experiment. Below 80 GeV, the processes $HH \to f\bar{f}$ can give proper annihilation cross sections using the Higg boson mediated diagram, at the same time with avoiding the constraints from direct searches by choosing the hHH coupling constant λ_H as an appropriate value. Here, we have assumed the mass of the Higgs boson to $m_h = 126$ GeV. When the LIP is below 63GeV, the collider signatures would not change qualitatively as well, however, the discovery channel of the new physics signal would be the invisible decay of the Higgs-boson at the LHC. We study the case where the masses of H and A are close to each other (I, III) for which the LEP and LHC experiments can not probe [10, 20–23]. The other cases are when $m_A - m_H$ is medium (II) or large such that the Z-boson from $A \to HZ$ becomes on-shell (IV). For the W-bosons in $H^\pm \to W^\pm H$, we consider the off-shell (I, II) and on-shell (III, IV) cases.

λ_2 and λ_H do not enter in our collider analysis. λ_H can be determined by the relic abundance which should be consistent with the recent WMAP search result [5] and also the bounds on the cross section of dark matter direct production. On the other hand, the method to determine λ_2 has not yet been established.

For our four benchmark points, the production cross sections of inert scalars at the ILC are large enough to be tested. In Table I, we also list the cross sections of HA production and H^+H^- production at $\sqrt{s} = 250$ GeV and 500 GeV. The cross section of HA production takes the largest value, i.e. 186 fb at $\sqrt{s} = 190$ GeV, 78 fb at $\sqrt{s} = 280$ GeV, and 46 fb at $\sqrt{s} = 350$ GeV in the cases (I, III), (II), and (IV), respectively. The cross section of H^+H^- production takes the largest value, i.e. 96 fb at $\sqrt{s} = 380$ GeV and 53 fb at $\sqrt{s} = 500$ GeV for the cases (I, II) and (III, IV), respectively. At $\sqrt{s} = 1$ TeV, the production cross sections are about 10 fb and 20 fb for HA production and H^+H^- production, respectively, for all the four benchmark points. For the cases (II, IV), $H^\pm$ decays into $W^\pm H$ predominantly, where we admit the W-boson to be off-shell if $m_{H^\pm} - m_H < m_W$. While for the cases (I) and (III), $H^\pm \to W^\pm A$ decay would be sizable as well, with the branching ratios about 32% and 27%, respectively. The decay of the A-boson is dominated by $A \to Z^{(*)}H$.

There are two important effects in the property of the SM-like Higgs boson, the invisible decay [20, 34] and the charged scalar loop contribution to the two-photon decay amplitude [11, 34, 35]. The invisible decay mode opens if $m_h > 2m_H$. If this is the case, the branching ratio for the invisible decay mode can be typically several tens percent [20, 34]. Thus, it could be discovered at the LHC [36]. The two-photon branching ratio of the SM-like Higgs boson can be directly related to $R_{\gamma\gamma} = \sigma(pp \to h \to \gamma\gamma)/\sigma(pp \to h \to \gamma\gamma)_{\rm SM}$, because the production cross-section of the Higgs-boson at the LHC is not modified in the IDM. It is shown [34] that $R_{\gamma\gamma}$ can be enhanced with relatively light $H^\pm$ ($m_{H^\pm} \lesssim 130$ GeV), negative λ_3 and no invisible decays.

III. COLLIDER SIGNATURES IN THE IDM AT THE ILC

In this section, we perform the simulation studies for the detection and the mass determination of the inert scalars in the IDM at the ILC. The kinematical distributions are calculated by using `MadGraph` [37] at the parton level with basic cuts for event generations. For charged leptons, we set $p_T^\ell > 1$ GeV, $|\eta_\ell| < 2.5$ and $\Delta R_{\ell\ell} > 0.2$ for the isolation requirement, where p_T is the transverse momentum, η is the pseudo-rapidity, and $\Delta R (= \sqrt{\Delta\eta^2 + \Delta\phi^2})$ is the distance of the two particle in the $\eta - \phi$ plane. For jets, we restrict ourselves with $p_T^j > 5$ GeV, $|\eta_j| < 2.5$ and $\Delta R_{jj}, \Delta R_{\ell j} > 0.4$. Furthermore, we require the missing transverse energy $\not{E}_T$ to be greater than 10 GeV to reduce background events from two photon scattering processes. The two photon scattering processes and QED radiation effects are not estimated in our analysis.

We note that, these cuts may be rather conservative, so that our parton level analysis makes sense. At e^+e^- colliders, hadronic final-states would be utilized even if they do not

	Inert scalar masses			ILC cross sections [$\sqrt{s} = 250$ GeV (500 GeV)]	
	m_H [GeV]	m_A [GeV]	$m_{H^\pm}$ [GeV]	$\sigma_{e^+e^- \to HA}$ [fb]	$\sigma_{e^+e^- \to H^+H^-}$ [fb]
(I)	65.	73.	120.	152. (47.)	11. (79.)
(II)	65.	120.	120.	74. (41.)	11. (79.)
(III)	65.	73.	160.	152. (47.)	0. (53.)
(IV)	65.	160.	160.	17. (35.)	0. (53.)

TABLE I. Masses of inert scalars and ILC cross sections for our four benchmark points.

form narrow jets. Then, the cuts on p_T and the isolation for partons may not be necessary. We include these cuts so that the number of jets in an event can be more easily accounted the number of outgoing partons in the processes. In case we loose these cuts, the number of available events would increase, but we expect more background contributions from the events with less partons. An isolation requirements for leptons may be weakened as well in the real experiment.

A. $e^+e^- \to HA$ process

First, we consider the HA production process followed by $A \to Z^{(*)}H$ decay. Since H is neutral and stable, it escapes from detection. Thus, it gives the signature with a dilepton (dijet) plus large missing energy. Expected background contributions come from dilepton (dijet) plus two neutrinos production in the SM.

First we study the collider signature of these events at $\sqrt{s} = 250$ GeV, for the parameter sets (I, III) and (II) where A decays into H and off-shell Z-boson. To reduce the SM background contributions, we apply following kinematical cuts; the scaled acoplanarity $\bar{\phi}_{\rm acop}$, which is the acoplanarity[2] multiplied by the sine of the smallest angle between a lepton (jet) and the beam axis, is larger than 100°; $|\cos\theta_{\ell\ell}| < 0.8$ for dilepton or $|\cos\theta_{jj}| < 0.6$ for dijet, where $\theta_{\ell\ell(jj)}$ is the polar angle of the dilepton (dijet) 3-momenta.

In the top left (right) panel in Fig. 1, we see the dilepton (dijet) energy distributions for the signal and background processes at $\sqrt{s} = 250$ GeV with the integrated luminosity of $\mathcal{L}_{\rm int} = 250$ fb^{-1}. After the cuts described above, background events are well reduced. The difference of the number of the signal events in dilepton and dijet signature comes from the branching ratio of the Z-boson, and that of the background events comes from the absence of WW production in the dijet case.

The endpoints of the $E_{\ell\ell(jj)}$ distribution are related with the masses of H and A as

$$E^{\rm max/min}_{\ell\ell(jj)} = \frac{\sqrt{s}}{4}\left(1 - \frac{m_H^2}{m_A^2}\right)\left[1 - \frac{m_H^2}{s} + \frac{m_A^2}{s} \pm \lambda(1, \frac{m_H^2}{s}, \frac{m_A^2}{s})\right], \tag{5}$$

where $\lambda(a,b,c) = \sqrt{a^2+b^2+c^2-2(ab+bc+ca)}$. Thus, the masses can be determined by measuring these endpoints. Since the distribution is quite steep around the maximum value,

[2] The acoplanarity angle $\phi_{\rm acop}$ is defined as the supplement of the difference of azimuthal angles of the leptons (jets).

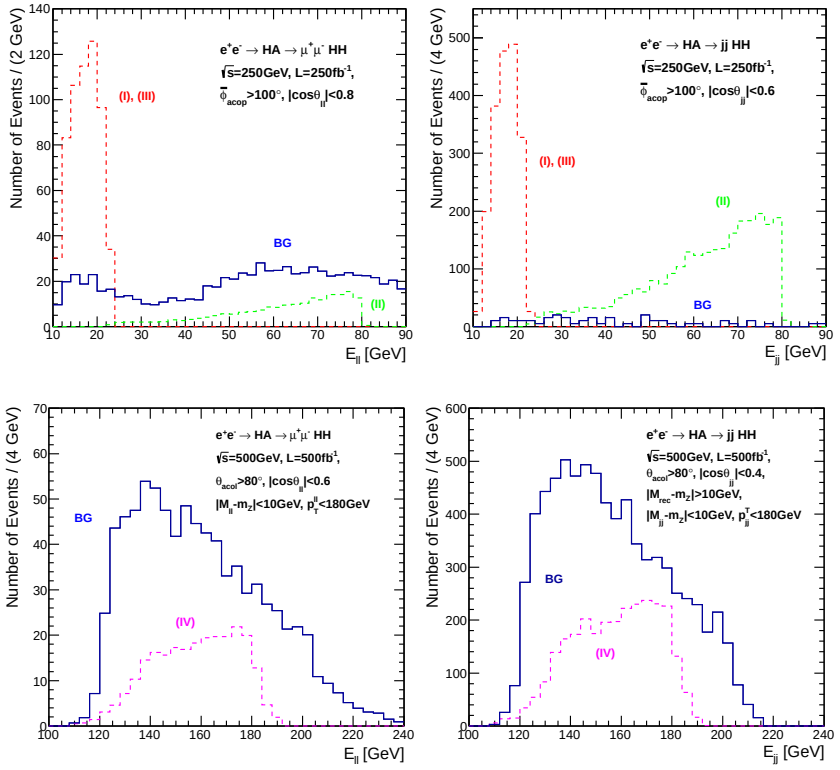


FIG. 1. Distributions of dilepton (dijet) energy in dilepton (dijet) plus missing energy event at the ILC with $\sqrt{s} = 250$ GeV and $\mathcal{L}_{\rm int} = 250$ fb^{-1} (top), and with $\sqrt{s} = 500$ GeV and $\mathcal{L}_{\rm int} = 500$ fb^{-1} (bottom).

$E^{\rm max}_{\ell\ell(jj)}$ should be a good observable to be measured precisely. It becomes 24 GeV even for the cases with small mass splitting (I, III), and 80 GeV for the case (II) at $\sqrt{s} = 250$ GeV. On the other hand, $E^{\rm min}_{\ell\ell(jj)}$ measurement may be difficult since the distribution is gradual around the minimum, and $E^{\rm min}_{\ell\ell(jj)}$ is too small for the cases (I, III) [$E^{\rm min}_{\ell\ell(jj)} = 2.4$ GeV at $\sqrt{s} = 250$ GeV].

In the bottom left (right) panel in Fig. 1, we show the $E_{\ell\ell(jj)}$ distributions for the parameter set (IV) with $\sqrt{s} = 500$ GeV and $\mathcal{L}_{\rm int} = 500$ fb^{-1}. To reduce SM background contributions, kinematical cuts are applied; $\theta_{\rm acol} > 80^\circ$ where the acollinearity angle $\theta_{\rm acol}$ is defined as the supplement of the opening angle of the dilepton (dijet); $|M_{\ell\ell(jj)} - m_Z| < 10$ GeV; $p_T^{\ell\ell(jj)} < 180$ GeV; $|\cos\theta_{\ell\ell}| < 0.6$ for the dilepton case, or $|\cos\theta_{jj}| < 0.4$ and $|M_{\rm rec} - m_Z| > 10$ GeV for the dijet case, where $M_{\rm rec}$ is the recoil mass defined as the invariant mass of the missing 4-momenta. In the case with the on-shell Z-boson, information of

the masses can be obtained from the endpoints of the $E_{\ell\ell(jj)}$ distribution as

$$E^{\rm max/min}_{\ell\ell(jj)} = \gamma_A \hat{E} \pm \beta_A \gamma_A \hat{p}, \tag{6}$$

where $\hat{E} = (m_A^2 - m_H^2 + m_Z^2)/(2m_A)$, $\hat{p} = m_A/2 \cdot \lambda(1, m_H^2/m_A^2, m_Z^2/m_A^2)$, $\gamma_A = (s - m_H^2 + m_A^2)/(2\sqrt{s}m_A)$ and $\beta_A\gamma_A = \sqrt{s}/(2m_A) \cdot \lambda(1, m_H^2/s, m_A^2/s)$. In spite of the finite-width effect of the Z-boson, the endpoints would be seen as sharp edges of the signal plateau. For the case (IV), the maximum and minimum of the dilepton (dijet) energies are $E^{\rm min}_{\ell\ell(jj)} = 134$ GeV and $E^{\rm max}_{\ell\ell(jj)} = 181$ GeV at $\sqrt{s} = 500$ GeV. The signal and background distributions are similar for both the dilepton and dijet cases, while the expected number of events are 10 times larger for the dijet case than that for the dilepton case. Thus, the statistical errors are small in the hadronic signature. On the other hand, the systematical errors would be negligible in the dilepton case due to the fine resolution of the lepton momentum measurement.

For the case with the off-shell Z-boson, from the maximum of the dilepton (dijet) invariant-mass distribution, the difference of the two scalar masses can be determined as

$$M^{\rm max}_{\ell\ell(jj)} = m_A - m_H. \tag{7}$$

We note that, for the case with small mass splitting, the measurement would be affected by QED radiation backgrounds and acceptance cuts.

B. $e^+e^- \to H^+H^-$ process

We here turn to the H^+H^- pair production, where $H^\pm$ predominantly decays into $HW^\pm$, and $W^\pm$ further into $\ell^\pm\nu$ or $q\bar{q}'$. We study the semi-leptonic and all-hadronic decay modes as successful signatures.

First, we study the semi-leptonic decay mode, where the signature is a charged lepton plus dijet plus large missing energy. The expected leading background process is $\tau^\pm\nu jj$ production followed by the leptonic decay of τ. The $\ell^\pm\nu jj$ background process can be reduced by requiring a large recoil mass in the event. The contribution from production of $\mu^+\mu^- jj$ and missing particles, where one of the muons goes out of the acceptance region, also turns out to be negligible. The event simulation for the case (I) [the case (III)] is the same as that for the case (II) [the case (IV)], but the overall normalization is multiplied by about a half, which is the square of the $H^\pm \to W^\pm H$ branching ratio, 68% [73%].

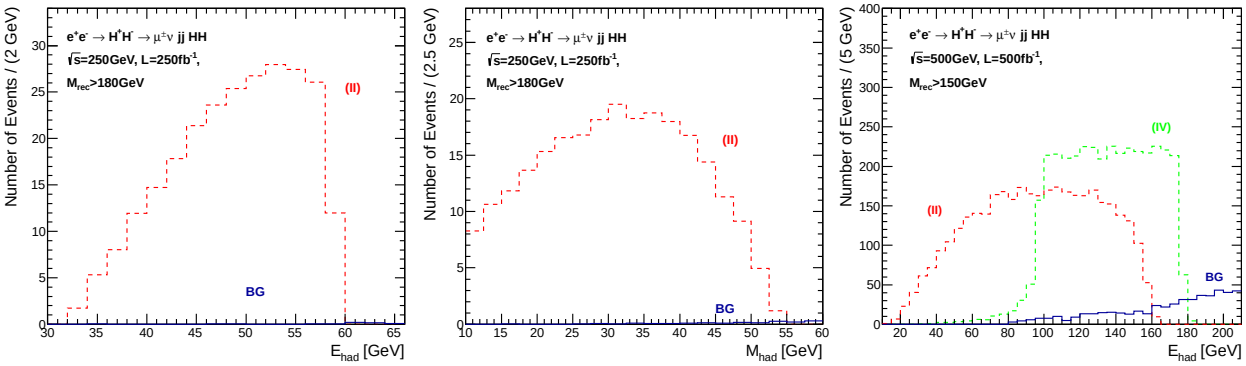


FIG. 2. Distributions of $E_{\rm had}$, $M_{\rm had}$ in the semi-leptonic decay mode at $\sqrt{s} = 250$ GeV with $\mathcal{L}_{\rm int} = 250$ fb^{-1} (left and middle) and that of $E_{\rm had}$ at $\sqrt{s} = 500$ GeV with $\mathcal{L}_{\rm int} = 500$ fb^{-1} (right).

In the left and middle panels in Fig. 2, distributions of $E_{\rm had}$ and $M_{\rm had}$ in the semi-leptonic decay mode are plotted by using the parameter set (II) at the ILC with $\sqrt{s} = 250$ GeV and $\mathcal{L}_{\rm int} = 250$ fb^{-1} with a cut of $M_{\rm rec} > 180$ GeV. The background contribution is negligible.

For the case with the off-shell W-boson, the endpoints of the all-jets (hadrons) energy distribution are given by

$$E_{\rm had}^{\rm max/min} = \frac{\sqrt{s}}{4}\left(1 - \frac{m_H^2}{m_{H^\pm}^2}\right)\left[1 \pm \sqrt{1 - \frac{4m_{H^\pm}^2}{s}}\right]. \tag{8}$$

Here, we note that the invariant mass of all hadrons vanishes at the endpoints. Therefore, the hadronic system would be actually observed as one jet near the endpoints. When we apply a cut on the smallest of the dijet invariant-mass at $M_{\rm cut}$, the endpoints of the energy distribution would be replaced by

$$E_{\rm had}^{\rm max/min} = \gamma_{H^\pm}\hat{E}_{\rm had} \pm \gamma_{H^\pm}\beta_{H^\pm}\,\hat{p}_{\rm had}, \tag{9}$$

with $\gamma_{H^\pm} = \sqrt{s}/(2m_{H^\pm})$, $\beta_{H^\pm} = (1 - 4m_{H^\pm}^2/s)^{1/2}$, $\hat{E}_{\rm had} = (m_{H^\pm}^2 - m_H^2 + M_{\rm cut}^2)/(2m_{H^\pm})$ and $\hat{p}_{\rm had} = m_{H^\pm}/2 \cdot \lambda(1, m_H^2/m_{H^\pm}^2, M_{\rm cut}^2/m_{H^\pm}^2)$. Thus, the mass information can be still obtained. Furthermore, the maximum value of the invariant mass of all hadrons is just the difference between $m_{H^\pm}$ and m_H,

$$M_{\rm had}^{\rm max} = m_{H^\pm} - m_H. \tag{10}$$

In the right panel in Fig. 2, the $E_{\rm had}$ distribution in the semi-leptonic decay modes are plotted by using the parameter sets (II) and (IV) at the ILC with $\sqrt{s} = 500$ GeV and

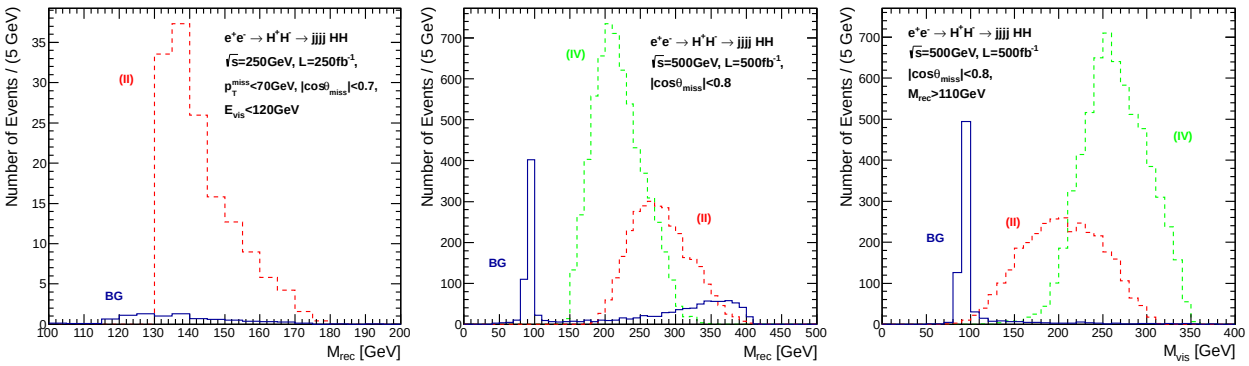


FIG. 3. Distributions of $M_{\rm rec}$ in the all-hadronic decay mode at $\sqrt{s} = 250$ GeV with $\mathcal{L}_{\rm int} = 250$ fb^{-1} (left), and $M_{\rm rec}$ and $M_{\rm vis}$ distributions in the all-hadronic mode at $\sqrt{s} = 500$ GeV with $\mathcal{L}_{\rm int} = 500$ fb^{-1} (middle and right).

$\mathcal{L}_{\rm int} = 500$ fb^{-1} with a cut of $M_{\rm rec} > 150$ GeV. Notice that the parameter set (II) corresponds to the case where $H^\pm$ decays into off-shell W and H, and (IV) corresponds to the case where $H^\pm$ decays into on-shell W and H. When the W-boson is on-shell, the signal distribution is like a rectangle where the edges are given by $E_{\rm had}^{\rm max/min}$ in Eq. (9), but with $M_{\rm cut}$ being replaced by m_W.

We note that the dijet system in the semi-leptonic decay mode may be replaced by the dijet subsystem which satisfies $M_{jj} \simeq m_W$ in the all-hadronic decay mode where the signature is four jets plus missing energy (see below).

Now, we turn to the all-hadronic decay mode, which results into the signature of four jets plus large missing energy. Major SM background comes from the production of four partons and two neutrinos. In the left panel of Fig. 3, $M_{\rm rec}$ distribution is plotted for the signal process using the parameter set (II) at $\sqrt{s} = 250$ GeV with $\mathcal{L}_{\rm int} = 250$ fb^{-1}. To reduce the SM background, kinematical cuts of $p_T^{\rm miss} > 70$ GeV, $|\cos\theta_{\rm miss}| < 0.7$ and $E_{\rm vis} < 120$ GeV are applied, where $\theta_{\rm miss}$ is the polar angle of the missing 3-momenta and $E_{\rm vis}$ is the sum of the energy of all hadrons in one event. As a result, the SM background is sufficiently reduced. The minimum of the $M_{\rm rec}$ distribution is at the twice of m_H,

$$M_{\rm rec}^{\rm min} = 2m_H. \tag{11}$$

In the middle panel of Fig. 3, the same distributions are plotted but for the signal processes using parameter sets (II) and (IV) at $\sqrt{s} = 500$ GeV with $\mathcal{L}_{\rm int} = 500$ fb^{-1}. By the

kinematical cut of $|\cos\theta_{\rm miss}| < 0.8$, the SM background is sufficiently reduced except at $M_{\rm rec} \simeq m_Z$. As it is shown in Appendix, the peak of the signal distribution is given by

$$M_{\rm rec}^{\rm peak} = \frac{m_H\sqrt{s}}{m_{H^\pm}}. \tag{12}$$

It is the advantage of this observable that this relation holds even when the W-boson in $H^\pm \to W^\pm H$ is off-shell. Thus, the ratio of m_H and $m_{H^\pm}$ can be determined.

In the right panel of Fig. 3, the $M_{\rm vis}$ distributions are plotted for the signal processes using parameter sets (II) and (IV) at $\sqrt{s} = 500$ GeV with $\mathcal{L}_{\rm int} = 500$ fb^{-1}. In addition to the kinematical cut applied in the previous panel, the cut of $M_{\rm rec} > 110$ GeV is applied to reduce the SM background which has a missing energy from $Z \to \nu\bar{\nu}$. After these cuts, the SM background is sufficiently reduced except at $M_{\rm vis} \simeq m_Z$. The signal distribution has a peak at

$$M_{\rm vis}^{\rm peak} = \frac{m_W\sqrt{s}}{m_{H^\pm}}, \tag{13}$$

when the W-boson in $H^\pm \to W^\pm H$ is on-shell [the case (IV)]. When the W-boson is off-shell, the relation on the peak position no more holds.

C. Mass Determination

Here, we summarize the observables for determining the masses of inert scalars. First, we consider the determination of $m_{H^\pm}$ and m_H in the process $e^+e^- \to H^+H^-$. If $m_{H^\pm} - m_H < m_W$, $m_{H^\pm}$ and m_H can be determined simultaneously by measuring the four quantities; $E_{\rm had}^{\rm max}$, $E_{\rm had}^{\rm min}$ in Eq. (8), $M_{\rm had}^{\rm max}$ in Eq. (10) and $M_{\rm rec}^{\rm min}$ in Eq. (11). In the left panel of Fig. 4, we show how the masses are determined by the measurements of the four quantities for the cases (I) and (II) at $\sqrt{s} = 250$ GeV. The four bands are plotted on the $m_{H^\pm}$-m_H plane by assuming that the four quantities are measured in ± 2 GeV accuracy (without any systematic shifts). For this assumption, the accuracy of the $m_{H^\pm}$ (m_H) determination would be ± 2 GeV (± 1 GeV). We note that our assumption is a simplest example in order to clarify the relation between the accuracy of the mass determination and that of the observables without involving experimental details. If the accuracy of the observable is changed, the width of the band on the figure varies in proportion to that. On the other hand, if $m_{H^\pm} - m_H \geq m_W$, the four observables, $E_{\rm had}^{\rm max}$, $E_{\rm had}^{\rm min}$ in Eq. (9) but with replacing

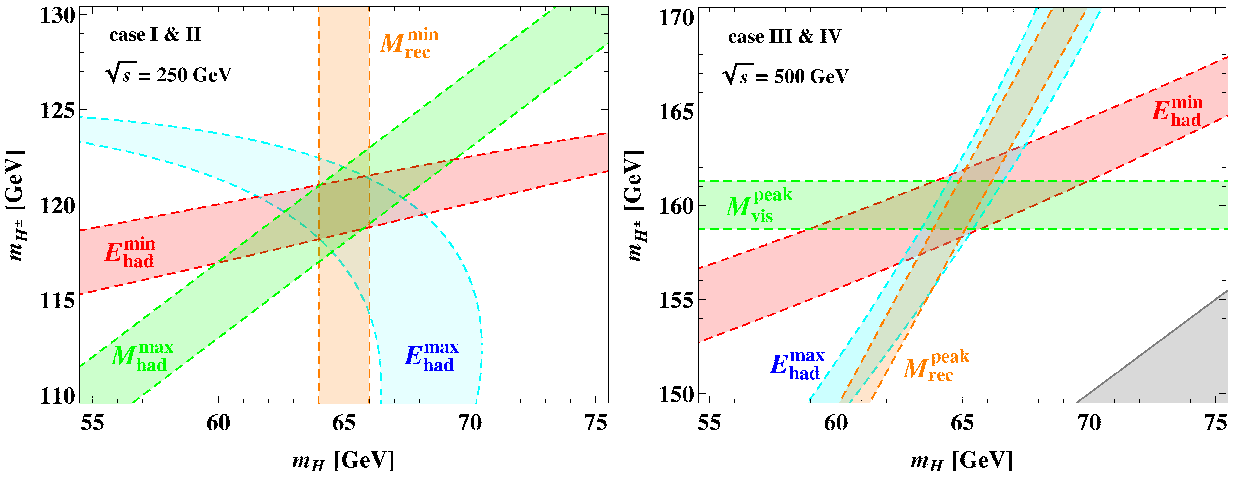


FIG. 4. Determinations of $m_{H^\pm}$ and m_H by the four observables are illustrated in the left [right] panel for the cases (I, II) [(III, IV)] at $\sqrt{s} = 250$ GeV [500 GeV]. Each observable is assumed to be measured in ± 2 GeV accuracy.

$M_{\rm cut}$ by m_W, $M_{\rm rec}^{\rm peak}$ in Eq. (12) and $M_{\rm vis}^{\rm peak}$ in Eq. (13) are utilized for the mass determination. In the right panel of Fig. 4, the four bands are plotted on the $m_{H^\pm}$-m_H plane by assuming that the four observables are measured in ± 2 GeV accuracy. It turns out that the constraints from measurements of $M_{\rm vis}^{\rm peak}$ and $M_{\rm rec}^{\rm peak}$ are more stringent than those from the $E_{\rm had}^{\rm max/min}$ measurements, if these quantities are measured in an equal accuracy. It is expected that peak positions can be precisely determined more than endpoints of distributions in the presence of the resolution of energy measurements and the remaining background contributions. By combining the four measurements with the uncertainty of ± 2 GeV, $m_{H^\pm}$ and m_H can be determined in ± 1 GeV accuracy.

Next, the determination of m_A can be achieved by combining the observables in the process $e^+e^- \to HA$. For the cases with the off-shell Z-boson (I, II, III), $E_{\ell\ell(jj)}^{\rm max}$ in Eq. (5) and $M_{\ell\ell(jj)}^{\rm max}$ in Eq. (7) measurements can be utilized. However, at $\sqrt{s} = 250$ GeV and $\sqrt{s} = 500$ GeV, since the two constraints are very similar, these masses cannot be determined at one point. In that case, one needs the value of m_H fixed in the process $e^+e^- \to H^+H^-$ as an input to determine m_A. While for the case with the on-shell Z-boson (IV), measurements of $E_{\ell\ell(jj)}^{\rm max/min}$ in Eq. (6) can be utilized. In that case, the expected accuracy of the mass determination is ± 3 GeV for the measurement of the observables in ± 2 GeV accuracy.

IV. DISCUSSIONS

At the ILC, another important measurement which we have not discussed is the spin measurement of the extra particles. In contrast to $H^{\pm}$ and (H, A) in the IDM, supersymmetric model contains charginos and neutralinos which are fermions, and the littlest Higgs model with T-parity or models with extra-dimension scenario predict heavy W-bosons and heavy photons which are vector particles. Since the production and decay of these particles can mimic the signatures studied in this letter, it is particularly crucial to discriminate models by the spin measurement of new particles. The spin of new particles could be traced in the threshold behavior of the production cross sections, the scattering angular dependence, and the decay angular dependence. It has been discussed that these measurements are possible for the processses we considered at the ILC [28, 38, 39]. On the contrary, those measurements at the LHC are difficult, because the center-of-mass energy in the partonic scattering is not fixed and also the center-of-mass system of the partonic scattering cannot be reconstructed.

Finally, we comment on the total comparison for the IDM studies at the LHC and the ILC. It is shown that the LHC has discovery potential for the inert scalars by using the signatures with multileptons plus large missing transverse momentum [10, 22, 23], if the mass difference is sufficiently large. Thus, in some preferable situations, the evidence of the inert scalars would show up at the LHC before the ILC experiment starts. On the other hand, as we have shown, the ILC can probe the case with smaller mass difference still in a good accuracy, as long as the production processes are kinematically accessible, i.e. $\sqrt{s} > 2m_{H^{\pm}}$ and $m_H + m_A$. Thus, there is a parameter region where any evidence can not be observed at the LHC, but the ILC could find it. In any case, at the ILC, the masses of the inert scalars can be reconstructed in good accuracy, and furthermore, the spin of the particles can be measured in principal. Therefore, the final discrimination of the model beyond the SM would be performed at the ILC.

V. CONCLUSIONS

To conclude, we have studied the collider phenomenology of the inert scalar particles at the ILC in the IDM. The model contains a scalar dark matter candidate which is stable

due to the unbroken Z_2 symmetry, in addition to another neutral scalar and charged scalar bosons. At collider experiments, because the dark matter would escape from the detector, the signatures always include large missing energy. We have studied the collider signatures of the pair production of the charged scalars and the associated production of the two neutral scalars with appropriate kinematical cuts to reduce the SM backgrounds. We have also investigated the observables to determine the masses of the scalars in these processes. We have shown that distinctive signatures can be observed even if the cases with small mass difference by applying simple kinematical cuts, and that by combining these observables the inert scalar masses can be reconstructed in a good accuracy at the ILC.

ACKNOWLEDGMENTS

M.A. thanks L. Lopez Honorez for useful discussions. S.K. and H.Y. would like to thank Keisuke Fujii for useful discussions. The paper was supported in part by Grant-in-Aid for Scientific Research, No. 24340036. M.A. was also supported in part by Grant-in-Aid for Scientific Research, No. 22740137. S.K. was also supported in part by Grant-in-Aid for Scientific Research, Nos. 22244031 and 23104006.

APPENDIX: INVARIANT-MASS DISTRIBUTIONS IN $X \to AA \to BCBC$

Here, we consider the kinematics of a general process $X \to A_1 A_2 \to B_1 C_1 B_2 C_2$, where X is a certain initial-state with the fixed collision energy, A_i are scalars with the same mass m_A, e.g. the identical particles or the charge-conjugate particles. B_i and C_i are any particles with their masses m_B and m_C, respectively, which are produced from the isotropic decay of A_i. For the meantime, we consider the case where all the particles are on-shell, i.e. $\sqrt{s} \geq 2m_A \geq 2m_B + 2m_C$. We consider the invariant-mass distribution of the $B_1 B_2$ pair:

$$\frac{d\sigma}{dM_{BB}^2} \propto \int d\Phi_4(X; B_1 C_1 B_2 C_2) \cdot \delta\left(M_{BB}^2 - (p_{B_1} + p_{B_2})^2\right) \times \frac{1}{[(p_{B_1} + p_{C_1})^2 - m_A^2]^2 + m_A^2 \Gamma_A^2} \cdot \frac{1}{[(p_{B_2} + p_{C_2})^2 - m_A^2]^2 + m_A^2 \Gamma_A^2}, \tag{A1}$$

where $d\Phi_n$ is the n-body phase-space volume element and Γ_A is the total decay width of A. Using the narrow width approximation for A, it is calculated as

$$\begin{aligned}\frac{d\sigma}{dM_{BB}^2} &\propto \int d\Phi_2(A_1; B_1C_1)\, d\Phi_2(A_2; B_2C_2)\, \delta\left(M_{BB}^2 - (p_{B_1} + p_{B_2})^2\right) \\ &\propto \int d\cos\theta_1 d\cos\theta_2 d\phi\, \delta\big(M_{BB}^2 - (p_{B_1} + p_{B_2})^2\big), \end{aligned} \tag{A2}$$

where $(\theta_1,\, \phi)$ and θ_2 are the decay angles in the rest-frame of A_1 and A_2, respectively. The azimuthal angle in the decay of A_2 is fixed to be zero, and the scattering angles in the process $X \to A_1A_2$, which are irrelevant to M_{BB}, are integrated out. By using the above integration variables, $(p_{B_1} + p_{B_2})^2$ is expressed as

$$\begin{aligned}&(p_{B_1} + p_{B_2})^2 = \\ &\qquad 2m_B^2 + \frac{s}{8}\left[\left(1+\beta_A^2\right)(\epsilon^2 + \beta^2 c_1c_2) + 2\beta_A\,\epsilon\beta(c_1+c_2) + (1-\beta_A^2)\beta^2 s_1 s_2 c_\phi\right]. \end{aligned} \tag{A3}$$

Here, $s = p_X^2$, $\beta_A = \sqrt{1-4m_A^2/s}$, $\epsilon = 1 + m_B^2/m_A^2 - m_C^2/m_A^2$, $\beta = \lambda(1, m_B^2/m_A^2, m_C^2/m_A^2)$ with $\lambda(a,b,c) = \sqrt{a^2+b^2+c^2-2(ab+bc+ca)}$, $c_i = \cos\theta_i$ for $i = 1, 2$ and $c_\phi = \cos\phi$. Although the numerical integration in Eq. (A2) is straightforward, we find that, unless $\sqrt{s} \simeq 2m_A$, it is a good approximation to neglect the last term in Eq. (A3). In that case, the M_{BB} distribution can be analytically expressed as

$$\frac{d\sigma}{dM_{BB}^2} \propto \log\left[\frac{4\left\{(s-2m_A^2)(M_{BB}^2-2m_B^2) - m_A^4\epsilon^2\right\}}{s^2\left\{(1+\beta_A^2)\beta - 2\beta_A\epsilon\right\}}\right], \tag{A4a}$$

for $M_{\rm min} \le M_{BB} \le m_B\sqrt{s}/m_A$, and

$$\frac{d\sigma}{dM_{BB}^2} \propto \log\left[\frac{s^2\left\{(1+\beta_A^2)\beta + 2\beta_A\epsilon\right\}}{4\left\{(s-2m_A^2)(M_{BB}^2-2m_B^2) - m_A^4\epsilon^2\right\}}\right], \tag{A4b}$$

for $m_B\sqrt{s}/m_A < M_{BB} \le M_{\rm max}$, where $M_{\rm max/min} = \sqrt{s}/2\cdot(\epsilon \pm \beta_A\beta)$. Thus, we find that the distribution has a peak at $m_B\sqrt{s}/m_A$, which therefore depends only on the ratio m_B/m_A but not on m_C.

Here we give some comments. In case with $m_A \le m_B + m_C$, if the particles C_i are off-shell, the peak position of the M_{BB} distribution is still given by $\sqrt{s}\, m_B/m_A$. On the other hand, if the particles B_i are off-shell, the reconstructed M_{BB} distribution is largely deformed. The M_{CC} distribution can be obtained by replacing $B \leftrightarrow C$ from the M_{BB} distribution in Eqs. (A4). Thus, the peak position of the M_{CC} distribution is given by $M_{CC}^{\rm peak} = m_C\sqrt{s}/m_A$, independently from m_B.

At e^+e^- colliders where the total 4-momenta of the collision can be fixed, it is possible to assess the invariant mass of the all missing particles (the recoil mass) by $M^2_{\rm rec} = (p_{\rm in} - p_{\rm vis})^2$, where $p_{\rm in}$ is the total 4-momenta of the initial e^+e^- system. Therefore, the invariant mass of the pair of two missing particles can be reconstructed, if these are the only missing particles in the event.

---

[1] G. Aad *et al.* [ATLAS Collaboration], Phys. Lett. B **716** (2012) 1.

[2] S. Chatrchyan *et al.* [CMS Collaboration], Phys. Lett. B **716** (2012) 30.

[3] N. G. Deshpande and E. Ma, Phys. Rev. D **18** (1978) 2574.

[4] R. Barbieri, L. J. Hall and V. S. Rychkov, Phys. Rev. D **74** (2006) 015007.

[5] L. Lopez Honorez, E. Nezri, J. F. Oliver and M. H. G. Tytgat, JCAP **0702** (2007) 028.

[6] M. Gustafsson, E. Lundstrom, L. Bergstrom, J. Edsjo and , Phys. Rev. Lett. **99**, 041301 (2007).

[7] E. M. Dolle and S. Su, Phys. Rev. D **80** (2009) 055012.

[8] L. Lopez Honorez and C. E. Yaguna, JHEP **1009** (2010) 046.

[9] L. Lopez Honorez and C. E. Yaguna, JCAP **1101** (2011) 002.

[10] M. Gustafsson, S. Rydbeck, L. Lopez-Honorez and E. Lundstrom, Phys. Rev. D **86** (2012) 075019.

[11] A. Goudelis, B. Herrmann and O. Stål, arXiv:1303.3010 [hep-ph].

[12] T. Hambye and M. H. G. Tytgat, Phys. Lett. B **659** (2008) 651.

[13] T. A. Chowdhury, M. Nemevsek, G. Senjanovic and Y. Zhang, JCAP **1202** (2012) 029.

[14] D. Borah and J. M. Cline, Phys. Rev. D **86** (2012) 055001.

[15] G. Gil, P. Chankowski and M. Krawczyk, Phys. Lett. B **717** (2012) 396.

[16] J. M. Cline and K. Kainulainen, Phys. Rev. D **87** (2013) 071701.

[17] E. Ma, Phys. Rev. D **73** (2006) 077301.

[18] E. Ma, Mod. Phys. Lett. A **21** (2006) 1777.

[19] D. Suematsu, T. Toma and T. Yoshida, Phys. Rev. D **79** (2009) 093004.

[20] Q. -H. Cao, E. Ma and G. Rajasekaran, Phys. Rev. D **76** (2007) 095011.

[21] E. Lundstrom, M. Gustafsson and J. Edsjo, Phys. Rev. D **79** (2009) 035013.

[22] E. Dolle, X. Miao, S. Su and B. Thomas, Phys. Rev. D **81** (2010) 035003.

[23] X. Miao, S. Su and B. Thomas, Phys. Rev. D **82** (2010) 035009.

[24] G. Abbiendi *et al.* [OPAL Collaboration], Eur. Phys. J. C **14** (2000) 187 [Erratum-ibid. C **16** (2000) 707].

[25] M. Acciarri *et al.* [L3 Collaboration], Phys. Lett. B **472** (2000) 420.

[26] J. Abdallah *et al.* [DELPHI Collaboration], Eur. Phys. J. C **31** (2003) 421.

[27] M. Aoki and S. Kanemura, Phys. Lett. B **689** (2010) 28.

[28] M. Asano *et al.*, Phys. Rev. D **84** (2011) 115003.

[29] S. Kanemura, T. Matsui and T. Nabeshima, Phys. Lett. B **723** (2013) 126.

[30] I. F. Ginzburg, K. A. Kanishev, M. Krawczyk and D. Sokolowska, Phys. Rev. D **82** (2010) 123533.

[31] P. Fayet, Nucl. Phys. B **78** (1974) 14.

[32] M. Gustafsson, PoS CHARGED **2010** (2010) 030.

[33] J. Beringer *et al.* [Particle Data Group Collaboration], Phys. Rev. D **86** (2012) 010001.

[34] B. Swiezewska and M. Krawczyk, arXiv:1212.4100 [hep-ph].

[35] A. Arhrib, R. Benbrik and N. Gaur, Phys. Rev. D **85** (2012) 095021.

[36] Y. Bai, P. Draper and J. Shelton, JHEP **1207** (2012) 192.

[37] J. Alwall, M. Herquet, F. Maltoni, O. Mattelaer and T. Stelzer, JHEP **1106** (2011) 128.

[38] S. Y. Choi, K. Hagiwara, H. -U. Martyn, K. Mawatari and P. M. Zerwas, Eur. Phys. J. C **51** (2007) 753.

[39] I. F. Ginzburg, arXiv:1211.2429 [hep-ph].